A Mechanically Intelligent and Passive Gripper for Aerial Perching and Grasping

HaoTse Hsiao, Jiefeng Sun ⬥, *Student Member, IEEE*, Haijie Zhang ⬥, and Jianguo Zhao ⬥, *Member, IEEE*

Abstract—Perching onto an object (e.g., tree branches) has recently been leveraged for addressing the limited flight time for flying robots. Successful perching needs a mechanical mechanism to damp out the impact and robustly grasp the object. Generally, such a mechanism requires actuation for grasping. In this article, we present a fully passive mechanism without using any actuator: a mechanically intelligent and passive (MIP) gripper that can be used for either aerial perching or grasping. Initially open, the gripper can be closed by the impact force during perching. After closure, if a sufficient mass (e.g., the robot's mass) is applied, the gripper can switch to a holding state and maintain that state to hold the mass. Once the mass is removed, the gripper can automatically open. We establish static models for the gripper to predict the required forces for successful state transitions. Based on the models, we develop design guidelines for the gripper so that it can be used for different flying robots with different weights. Experiments are conducted to validate the models. Attaching the gripper onto a quadcopter, we demonstrated aerial perching onto rods and aerial grasping rod-like objects. Because the MIP gripper is lightweight (can reach a mass ratio of 0.75% between the gripper and the grasped object for static grasping), we expect it would be well suited for aerial perching or grasping due to the limited payload capability for flying robotsxv.

Index Terms—Aerial perching, grasping, gripper, mechanical intelligence.

I. INTRODUCTION

BIOLOGICAL flyers (e.g., birds) can perch onto tree branches or power lines to rest, saving energy for flights [1], [2]. Inspired by biological flyers, perching has recently been leveraged for aerial robots, especially quadcopters, to address their limited flight time. After perching, they can
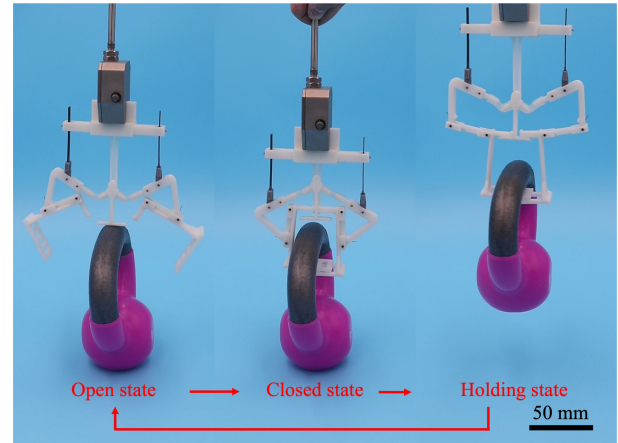

Fig. 1. MIP gripper passively grasps and lifts a 2.27 kg kettlebell (left: open state; middle: closed state; right: holding state). See the Supplementary Material for the grasping process.

still monitor a given area but without consuming energy required for staying airborne, enabling long-duration monitoring or surveillance. Successful perching necessitates two types of intelligence [3].

1) Computational intelligence, i.e., algorithms that can estimate, plan, and control the robot's motion [4], [5].
2) Physical intelligence [6], i.e., perching mechanisms that can damp out the perching impact and grasp the intended perching object [7].

While computational intelligence is critical for successful perching, properly designed mechanisms (e.g., grippers) with physical intelligence can enable perching without precise motion control, alleviating the burden for computational intelligence [8]. The embodiment of intelligence into a robot body has also been investigated for many other robotic systems, especially soft robots [9].

Recently, researchers have investigated the physical intelligence for perching by developing various perching mechanisms (recent comprehensive reviews in [1] and [10]). Since our gripper is intended for perching onto rod-like objects, we briefly review some representative designs for rod perching. Most designs for rod perching embody a gripper structure, and many of them require actuators (e.g., dc motor, servos, pneumatic pump) to either open or close the gripper [11]–[16]. Some designs are purely passive, relying on the drone's mass to close or open the gripper [17]–[19]. Besides the grippers, a grapple with

TABLE I
COMPARISON OF EXISTING GRIPPERS FOR ROD PERCHING

Existing grippers	Actuators	gripper weight	total weight	mass ratio	Task
Modular landing gears [3]	Servo	318 g	1438 g	22%	Perching
NTU gripper [11]	Servo	500 g	1800 g	28%	Perching
Avian-Inspired [17]	None	478 g	533 g	90%	Perching
Sarrus-Based [18]	None	20 g	204 g	10%	Perching
Bird Inspired [14]	Servo	89.2 g	567.2 g	16%	Perching
Microspine Grapple [20]	None	32 g	1766 g	2%	Perching
Passive Perching [21]	None	170 g	850 g	20%	Perching
Soft drone [22]	DC motor	200 g	1900 g	11%	Grasping
AGRASP [12]	Servo	372 g	2300 g	16%	Perching or grasping
Passive magnetic grasping [13]	Servo	292 g	770 g	38%	Grasping
Passive closing [15]	Servo	551 g	833 g	66%	Perching or grasping
Bistable [8]	DC motor	13 g	40 g	33%	Perching
MIP Gripper (This work)	**None**	**28 g**	**593 g**	**5%**	**Perching or grasping**

microspines has been investigated for perching onto different objects [20]. However, existing grippers used for both perching and grasping usually have a large mass compared with the robot's mass (mass ratio > 10%) due to the actuators. It remains largely unknown if it is possible to develop a fully passive gripper that can be used for both perching and grasping. Such a gripper can be lightweight without actuators and control circuits, allowing the robot to carry other useful payloads.

In this article, we present the design, analysis, and experiments for a mechanically intelligent and passive (MIP) gripper (see Fig. 1) for either aerial perching or grasping. With a mass of 28 g, the MIP gripper can passively grasp and hold a mass of 3.7 kg, enabling a mass ratio between the gripper and the object to be 0.75% for static grasping (see the Supplementary Material). Consider grasping as an example (the same principle applies to perching). The gripper initially stays at an open state (see the left-hand side of Fig. 1). When it contacts a kettlebell, it can close due to the contact force from the kettlebell's handle. In this closed state, the gripper encloses the kettlebell's handle (see the middle of Fig. 1). If the gripper is lifted up, it can hold the kettlebell with the holding state (see the right-hand side of Fig. 1). Finally, if the gripper is lowered down to let the kettlebell touch the ground, it can automatically open to release the kettlebell to return to the original open state.

We compare our MIP gripper with closely related grippers in Table I. The table suggests that the MIP gripper distinguishes itself in two aspects. First, it has a small mass ratio (5%) between the gripper and the flying robot. Second, the MIP gripper can be used for either perching when the gripper is installed at the top of a drone or grasping when installed at the bottom (see the last column in Table I), whereas most of the other designs only demonstrated a single task. Further, we can easily adjust a single element (see the details in Section III-C) in the gripper to allow for grasping or perching for flying robots with different weights and payload capabilities.

The MIP gripper is based on our recent bistable gripper [8], [23], which allows a quadcopter to passively perch onto a rod by directly using the impact force during perching. However, our previous gripper suffers from several problems. First, it is not fully passive, requiring a DC motor to open the gripper by actuating a lever mechanism, resulting in a complicated design with a large mass (mass ratio between the gripper and

the quadcopter is 33%). Second, even though we don't need to precisely control the perching process, we need to precisely control the releasing process. Once the gripper opens, we need to instantly turn on the drone's motors to generate upward thrust forces to prevent the drone from falling to the ground. Third, our previous gripper can only hold a small mass because a mass larger than the maximum switching force will open the gripper.

The MIP gripper can address the shortcomings of our previous bistable gripper.

1) It is fully passive by directly leveraging the impact force to close the gripper, the drone's mass to maintain the closed state, and a special design of extended fingers to open the gripper.
2) It does not need precise control for both perching and releasing. During releasing, we turn on the drone's motor first, after which the gripper will automatically open, simplifying the control process for releasing.
3) It can hold a large mass (132 times its own mass), making the gripper suitable for perching with heavy drones as well as grasping heavy objects.

The advantages of MIP gripper compared with our previous bistable gripper come from a significant redesign and analysis. First, we realize the fully passive design by using a pair of extended fingers with a latch and passive folding capability. The latch will enable the holding state to make the gripper remain closed and hold the mass when an external force is applied, whereas the passive folding capability allows the extended fingers to fold back to their original state when the external force is removed (detailed working principle in Section II). Because of the extended fingers, theoretical models for analyzing the forces are also different and more challenging. Second, we can adjust the forces required for perching or grasping by changing the length of two vertical beams in the gripper. This design enables the MIP gripper to be easily adjusted to perch for flying robots with different weights or grasp objects with different weights.

The main contribution of this article is twofold. First, we present a fully passive and adjustable gripper that can be used for different flying robots for aerial perching or grasping tasks. Such a mechanically intelligent gripper can alleviate the requirement for computational intelligence. Second, we establish theoretical models to predict the required forces for passively opening and closing the gripper. Based on the models, we establish a design
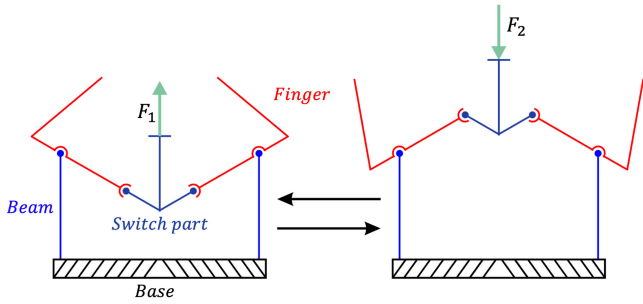
Fig. 2. Bistable mechanism with two stable states: top (right-hand side figure) and bottom (left-hand side figure). If the mechanism is initially at the bottom state, it can switch to the top stable state when F_1 is applied to the switch part. It can switch from top back to bottom state when F_2 is applied.

guideline for how to adjust the length of the vertical beam for different flying robots to allow successful perching or grasping.

The rest of this article is organized as follows. In Section II, we introduce the working principle and design of the MIP gripper. In Section III, we establish analytical models to predict the forces to open and close the MIP gripper. In Section IV, we conduct experiments to verify the models and also perform the grasping and perching experiments to demonstrate the gripper's capabilities. In Section V, we discuss the limitations of the MIP gripper and how to address the limitations. Finally, Section VI concludes this article.

II. DESIGN OF THE MIP GRIPPER

The MIP gripper can both open and close passively using a compliant mechanism [24]. This is accomplished by combining a bistable mechanism with a pair of extended fingers. In this section, we introduce the bistable mechanism in the gripper, design of the gripper, and its working principle.

A. Bistable Mechanism for the MIP Gripper

The MIP gripper is based on a bistable mechanism, as shown in Fig. 2. The bistable mechanism is made from a pair of vertical beams rigidly connected to a base. A pair of fingers is connected to the beams through revolute joints. The fingers are connected to a switch part in the middle via two compliant joints (CJs). With this design, the mechanism will have two stable states: top and bottom stable states. With the mechanism initially at the bottom stable state (see the left-hand side of Fig. 2), if an upward force F_1 is applied to the switch part, the beams will bend outward, and the mechanism will switch to the top stable state (see the right-hand side of Fig. 2). In this top state, if a downward force F_2 is applied to the switch part, the mechanism can switch back to the bottom stable state. A detailed investigation of the bistable mechanism can be found in [8].

B. Design of the MIP Gripper

The MIP gripper is developed based on the bistable mechanism. It consists of a rigid base, two adjustable vertical beams attached to the base, two fingers connected to the beams through
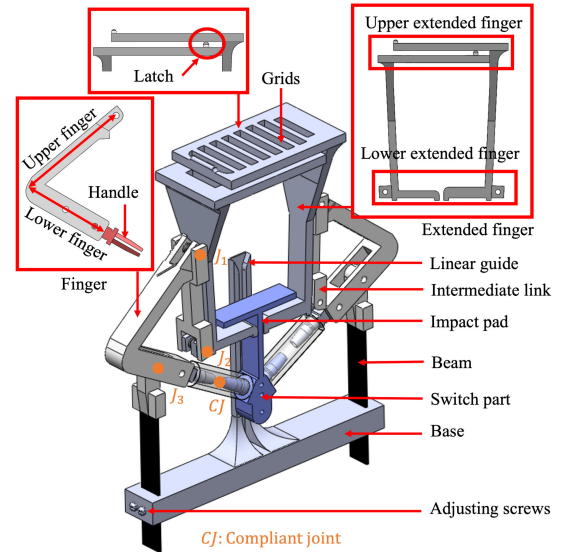

Fig. 3. Structure and key components of the MIP gripper.

a revolute joint (see J_3 in Fig. 3), two intermediate links connected to the fingers through another revolute joint (see J_1 in Fig. 3), two extended fingers connected to the intermediate links through revolute joint J_2, and a switch part connected to the fingers through two elastic tubes as CJs. If we don't have the two intermediate links and the two extended fingers, the remaining parts become the bistable mechanism discussed in Section II-A.

Because the motion of extended fingers is not constrained, we place a torsion spring at J_1 and J_2, respectively. Both springs are pretensioned so that the extended fingers can be folded to be in the open configuration when the bistable mechanism is at the top stable state.

Each of the two extended fingers includes an upper extended finger (UEF) and a lower extended finger (LEF) (see Fig. 3). The right UEF has some grids, whereas the left UEF has a protrusion that can insert into the grids for latching if an upward force is applied. But when no upward force is applied, the two UEFs are designed to be separate from each other (the left UEF is lower than the right UEF). The two LEFs are under the impact pad of the switch part so that they can contact the impact pad to remain in the holding state when an upward force is applied to the UEFs.

The length of the two vertical beams can be adjusted using two screws on the rigid base. This allows the gripper to be used for different flying robots (details on how to determine the beam's length will be discussed in Section III-C). We also designed a linear guide to ensure that the switch part can only move vertically without side movements. This guide is realized by using two small screws attached to the switch part, and the screws can slide along a groove in the guide.

C. Working Principle of the MIP Gripper

With the designed MIP gripper, we explain the working principle with a simplified sketch (see Fig. 4) using perching as an example (the same principle applies to grasping). Consider
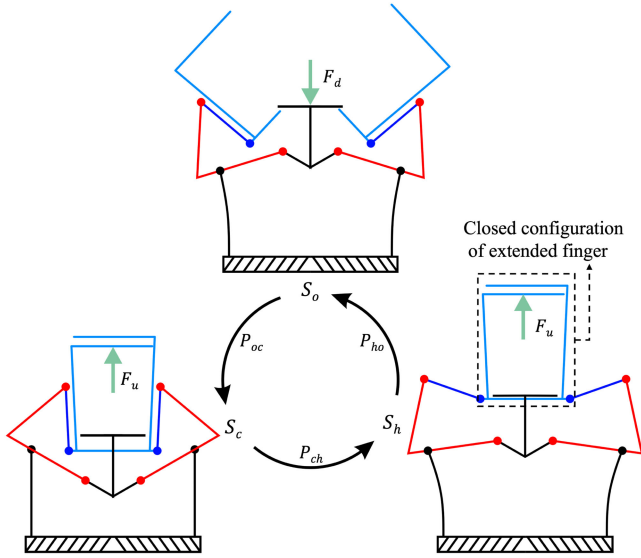
This article has been accepted for inclusion in a future issue of this journal. Content is final as presented, with the exception of pagination.

4   IEEE/ASME TRANSACTIONS ON MECHATRONICS

Fig. 4. Illustration of the MIP gripper's working principle. Top sketch: open state S_o; bottom-left sketch: closed state S_c; bottom-right sketch: holding state S_h.
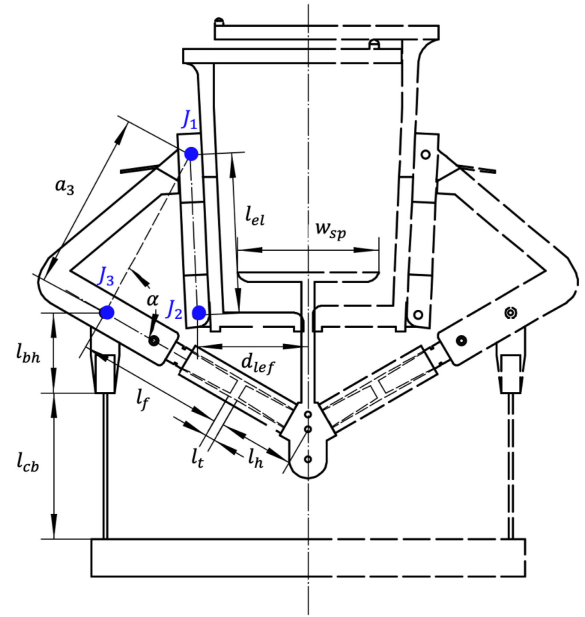

Fig. 5. Front view of the gripper. The geometric parameters are labeled in left half since the gripper is symmetrical with respect to its center.

the case when the gripper is placed on the top of a drone to allow it to perch onto a rod. Also, assume the gripper is initially open (state S_o, the top of Fig. 4). Starting from S_o, the gripper can switch to the closed state S_c (see the bottom left of Fig. 4), then to an holding state S_h (see the bottom right of Fig. 4), and finally return to the original open state S_o. In the following, we explain the transitions of the three states.

1) Process P_{oc} (From S_o to S_c): As the drone flies upward, the gripper will contact the rod, resulting in a downward force F_d applying on the switch part (see the top of Fig. 4). This F_d will switch the bistable mechanism to the bottom stable state S_c, closing the gripper to encircle the rod inside the two extended fingers.

2) Process P_{ch} (From S_c to S_h): With the rod inside the two extended fingers, we can turn OFF the motors of the drone. In this case, the drone's mass must be balanced by an upward force (F_u) applied to the extended figures (see the left-hand side of Fig. 4). This force F_u will first latch the two UEFs and push the extended fingers upward to switch the bistable mechanism to the top stable state. During this process, the extended fingers remain closed because the two UEFs are latched together due to F_u. Eventually, the gripper will be in an holding state S_h (see the right-hand side of Fig. 4). In this case, the drone can hang on the rod without any additional energy input.

3) Process P_{ho} (From S_h to S_o): When we turn on motors of the drone to generate thrust, the gripper can switch from S_h to S_o. During this process, the upward force (F_u) applied to the extended fingers disappears since the thrust can balance the drone's mass. The two UEFs can thus delatch from each other because they are designed to be separate from each other when no upward force is applied. Because of the torsional springs at joints J_1 and J_2, the extended fingers will fold back to their original configuration, opening the gripper to return to state S_o.

To ensure the successful switching between the three states S_o, S_c, and S_h, we need to have the following conditions.

1) *Process P_{oc} (from S_o to S_c):* The impact force F_d should be large enough to switch the state for the bistable mechanism. This means that the drone should have enough thrust force to generate the required impact force.
2) *Process P_{ch} (from S_c to S_h):* F_u should be large enough to switch the state of the bistable mechanism, and it can be quite large as long as the gripper does not break.
3) *Process P_{ho} (from S_h to S_o):* To ensure this process, the bistable mechanism should maintain its bistability, i.e., it should not go back to its initial bottom state.

All of these conditions will be used to develop a design guideline in Section III-C for obtaining the proper length for the vertical beams to ensure successful perching for different drones and grasping different weights.

III. MODELING OF THE MIP GRIPPER

To ensure successful switching of states, we need to predict how F_u on extended fingers will change with respect to the vertical displacement of the extended fingers (denoted as x), how F_d on the switch part will change with respect to the vertical displacement of the switch part (denoted as d), i.e., force profile $F_u(x)$ and $F_d(d)$. For perching, $F_d(d)$ will determine the minimum required impact force to close the gripper, and $F_u(x)$ will determine the minimum mass of the drone to open the gripper. In this section, we discuss how to solve $F_u(x)$ and $F_d(d)$ separately.

A. Profile for Upward Force on Extended Fingers: $F_u(x)$

Some fixed geometric parameters are shown in Fig. 5 for the MIP gripper in S_c. They will be explained later in this section.
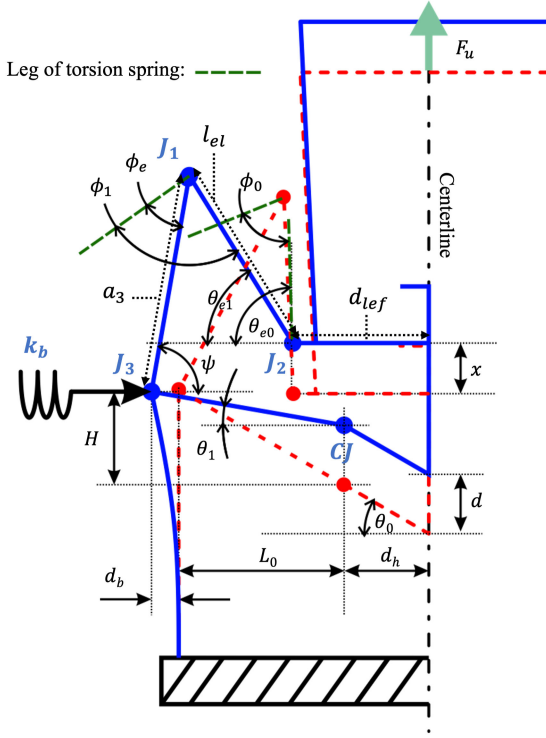
Fig. 6. Schematic showing the P_{ch}. The red dash lines represent the initial closed state (S_c), whereas the solid blue lines represent the gripper when the switch part moves up by a distance of d. Since the gripper is symmetrical, only half of the gripper is shown.

A diagram for the gripper during P_{ch} is shown in Fig. 6. The displacement of the extended finger in the vertical direction changes with respect to F_u during P_{ch}. Note that x is different from the displacement of the switch part d. F_u with respect to x during P_{ch} can be obtained using the Theorem of Least Work by considering the total strain energies (E_{tot}) as

$$F_u(x) = \frac{\partial E_{\text{tot}}}{\partial x} = \frac{\partial E_{\text{tot}}}{\partial d}\frac{\partial d}{\partial x} \qquad (1)$$

where $E_{\text{tot}} = E_b + E_t + E_{s1} + E_{s2}$, with E_b as strain energies in the two beams, E_t as strain energies in the two CJs, and E_{s1} and E_{s2} as strain energies in torsion springs placed at J_1 and J_2, respectively. Since the four strain energies can be easily represented in terms of d instead of x, we use d as an intermediate variable, and first take the derivative with respect to d: $F_u(d) = \partial E_{\text{tot}}/\partial d$, and then obtain $F_u(x)$ by multiplying $F_u(d)$ with $\partial d/\partial x$ [see (1)]. In the following, we derive the individual energies for E_b, E_t, E_{s1}, and E_{s2}. Then, we will solve $F_u(d)$ and $\partial d/\partial x$ to eventually obtain $F_u(x)$.

First, the total strain energy from two beams E_b can be approximated as two linear springs because of the small bending [8] as

$$E_b = k_d d_b{}^2 \qquad (2)$$

where k_d is the spring constant. d_b is the horizontal displacement of the bending beams that can be derived from a geometrical relationship: $H^2 + L_0{}^2 = (H-d)^2 + (L_0 + d_b)^2$, where H and L_0 are constants (see Fig. 6) at the initial configuration S_c that can be

obtained by: $H = (l_f + \gamma l_t)\sin\theta_0$ and $L_0 = (l_f + \gamma l_t)\cos\theta_0$, where θ_0 is the angle between the horizontal line and the lower finger at S_c. l_f is the length from J_3 to the end of lower finger's handle. l_t is distance between the handles of the lower finger and switch part, and γ is a ratio to locate bending point for the tube if we use a pseudorigid-body model to approximate the tube's bending [8]. Then, we can solve d_b as a function of d: $d_b = \sqrt{L_0{}^2 + 2Hd - d^2} - L_0$.

Second, the total strain energy of two CJs E_t is

$$E_t = k_\theta(\theta_1 - \theta_0)^2 \qquad (3)$$

where k_θ is the spring constant of the CJ, which can be experimentally obtained (see the details in Section IV) and $\theta_1 = \arctan\left[(H-d)/(L_0+d_b)\right]$ is the angle between the horizontal line and the lower finger at the CJ during the process P_{ch} (blue line).

Third, the torsion springs at J_1 have a prerotating angle ϕ_0 when the gripper is in the closed state S_c, and it will increase to ϕ_1 when the extended fingers move up for a displacement of x (see Fig. 6). The total strain energy E_{s1} of two springs at J_1s can be written as

$$E_{s1} = k_{s1}\phi_1{}^2 \qquad (4)$$

where k_{s1} is spring constant of the torsional spring, $\phi_1 = \pi - \theta_{e1} - \psi + \phi_e$ where ϕ_e is an angle between the leg of torsion spring and a virtual link connecting J_1 and J_3, $\theta_{e1} = \arccos[(d_b + L_0 + d_h - a_3\cos\psi - d_{\text{lef}})/l_{\text{el}}]$ is the angle between horizontal line and intermediate link, d_h is distance from the CJ to the centerline, l_{el} and d_{lef} are, respectively, the length of the intermediate link and the LEF, a_3 is the length of the virtual link between J_1 and J_3, $\psi = \alpha - \theta_1$ is the angle between the virtual link and horizontal line, and α is the angle between the virtual link and the lower finger.

Fourth, the torsion springs at J_2 also have a prerotating angle θ_{e0} which is between the horizontal line and intermediate link at S_c. The total strain energy of these two springs E_{s2} can be written as

$$E_{s2} = k_{s2}(\pi - \theta_{e1})^2 \qquad (5)$$

where k_{s2} is the spring constant of the torsional spring. The initial value of θ_{e1} is θ_{e0}.

Based on the individual energies, we can obtain E_{tot} to solve for $F_u(d) = \partial E_{\text{tot}}/\partial d$ in (1) as

$$F_u(d) = \frac{-2}{a_3\cos\psi + A\cot\theta_{e1}}\left[k_b d_b(H-d) + \frac{A}{l_{\text{el}}\sin\theta_{e1}}\right.$$
$$\left. \times (k_{s1}\phi_1 + k_{s2}(\pi - \theta_{e1})) - k_\theta(\theta_1 - \theta_0) - k_{s1}\phi_1\right] \qquad (6)$$

where $A = H - d + a_3\sin\psi$.

Finally, the relationship between d and x is required for solving $\partial d/\partial x$ in (1). Since we assume J_3 can only displace horizontally, x can be solved from the vertical distance between J_3 and J_2: $x = a_3\sin\psi - l_{\text{el}}\sin\theta_{e1} + d_{(J_3, J_2)}$, where $d_{(J_3, J_2)}$ is initial vertical distance between J_3 and J_2. Therefore, we can
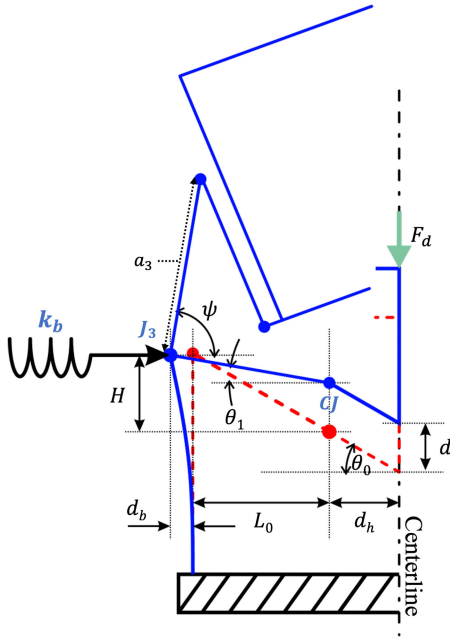
Fig. 7. Schematic showing P_{oc}. F_d will change with respect to d. The blue lines are corresponding to the open state and the red dashed lines are corresponding to the closed state.

obtain $\partial x / \partial d$ as

$$\frac{\partial x}{\partial d} = (L_0 + d_b)/[a_3 \cos \psi + \cot \theta_{e1}(H - d + a_3 \sin \psi)].$$

With $F_u(d)$ and $\partial x/\partial d$, we can plug them into (1) to solve for $F_u(x)$.

B. Profile for Downward Force on Switch Part: $F_d(d)$

During the process of P_{oc}, the downward force F_d applied to the impact pad can displace the pad to close the gripper. Note that intermediate links and extended fingers will not participate in the process because they are folded. In this case, we can simplify the sketch, as shown in Fig. 7. F_d with respect to d can still be solved from the total energy E_{tot} as

$$F_d(d) = \frac{\partial E_{tot}}{\partial d} \qquad (7)$$

where $E_{tot} = E_b + E_t$ with E_b the total strain energy from the beams and E_t the total strain energy from the tubes (derived in Section III-A).

Solving (7), we can obtain F_d with respect to d during P_{oc} as

$$F_d(d) = \frac{2}{L_0 + d_b}[k_d d_b (H - d) - k_\theta (\theta_1 - \theta_0)]. \qquad (8)$$

Unlike (6), (8) is simpler because we don't need to consider the extended fingers and the intermediate links since they are folded.

C. Design Guidelines of the MIP Gripper

Based on the profiles $F_u(x)$ and $F_d(d)$, we can develop design guidelines for the MIP gripper: how should we design the gripper so that it can successfully allow a drone to perch onto a rod or grasp a given payload. We aim to develop a framework

for designing an adjustable MIP gripper that can be used for different drones. Since there are many geometric parameters in the gripper, we simplify the design problem by choosing a parameter that can be easily adjusted while fixing all the other parameters. This parameter is the bending stiffness of the vertical beam k_b since it can be easily adjusted by changing its length using screws at the base (see Fig. 3).

We use perching to establish the design guidelines and discuss how to apply the guidelines to grasping at the end of this section. Assume a drone has a maximum thrust force of F_t and a mass of F_w. To enable successful perching using the MIP gripper, we need to guarantee the three conditions discussed at the end of Section II-C to allow successful state switching.

1) Process P_{ho} (From S_h to S_o): To ensure this process, the bistable mechanism should maintain its bistability so that when F_u is removed, the bistable mechanism can stay in the top stable state to allow the gripper to automatically open. According to the bistablity analysis in [8], k_b should be large enough. This means that for a given k_b, the maximum value of profile $F_d(d)$ should be positive. We denote this maximum value as $F_{d,\max}(k_b)$ since it changes with respect to k_b. Therefore, to ensure a successful transition from S_h to S_o, we have

$$F_{d,\max}(k_b) > 0 \qquad (9)$$

2) Process P_{oc} (From S_o to S_c): The impact force should be large enough to switch the state from S_o to S_c. This means k_b should be small enough so that the drone's maximum thrust force F_t can result in a sufficient impact force to switch the state. Since it is complicated to determine impact force dynamics, we simplify the problem by considering the maximum upward quasi-static force that can be generated by the drone, $F_t - F_w$, which represents the lower bound of the maximum impact force. Therefore, to ensure a successful transition from S_o to S_c, we have

$$F_{d,\max}(k_b) < F_t - F_w. \qquad (10)$$

3) Process P_{ch} (From S_c to S_h): In this process, k_b should also be small enough so that the drone's mass F_w can successfully switch the state from S_c to S_h. The maximum value of profile $F_u(x)$ [denoted as $F_{u,\max}(k_b)$] should be less than F_w. Therefore, we can have another inequality

$$F_{u,\max}(k_b) < F_w. \qquad (11)$$

With the three inequalities (9)–(11), we can numerically solve for a range for k_b given F_t, F_w, and other geometric parameters for the gripper. For instance, for the drone (593 g) that will be used in our experiments in Section IV, it has $F_w = 5.28$ N and a maximum thrust force of $F_t = 8.89$ N. If we use this drone for perching, we can use MATLAB to numerically find $420.7 < k_b < 2048$ Nm^{-1}.

The same design framework applies to aerial grasping when the gripper is placed at the bottom of a drone. To ensure successful grasping, (9) is the same since we still need to ensure the bistability. For (10), we need to consider two cases. If the drone needs to land on the ground to grasp, then $F_t - F_w$ should be changed to F_w since the drone will rely on its mass to switch the state from S_o to S_c. If the drone needs to grasp without landing on
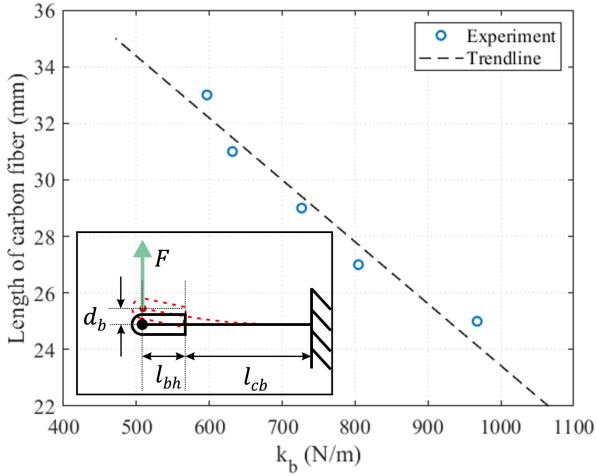
Fig. 8. Experimental results for the relationship between k_b and l_{cb} from experiment: $l_{cb} = -0.025k_b + 47.5$. The experimental setup is shown inside the plot.
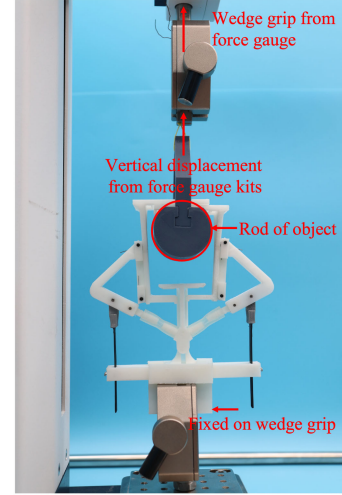

Fig. 9. Experimental setup for measuring the upward force during P_{ch}. The gripper is fixed on a wedge grip and a cylindrical rod connected the force gauge will drag the gripper to switch the state.

the ground, then $F_t - F_w$ should be changed to $F_w - F_{\text{minThrust}}$, where $F_{\text{minThrust}}$ is the additional thrust applied to keep the drone airborne. For (11), we need to change F_w to the mass of the object that will be grasped. For instance, if we want a drone to grasp an object of 260 g by landing on the ground, then, we can solve the three inequalities to get $420.7 < k_b < 661.2$ Nm^{-1}. Therefore, if we use the same gripper to be placed on a drone with a mass of 593 g for either perching or grasping an object of 260 g, then the range of k_b should be $420.7 < k_b < 661.2$ Nm^{-1}.

With the range of k_b, we can further determine the range of length of the vertical beams (see l_{cb} in Fig. 5), which can be adjusted using two screws in our design. Although we can obtain the analytical solution for k_b with respect to l_{cb}, we experimentally obtain such a relationship for better accuracy. Fig. 8 shows how k_b will change with respect to l_{cb} from 27 to 35 mm. Since l_{cb} is linear with respect to k_b, we can get the trend line function $l_{cb} = -0.025k_b + 47.5$ to get the corresponding l_{cb} for different k_b. Therefore, if we want to use the same gripper to allow for a drone weighing 593 g to perch or grasp an object weighing 260 g, the length of the vertical beam should be in a range $30.97 < l_{cb} < 36.98$ mm.

IV. EXPERIMENTS AND RESULTS

In this section, we elaborate on the fabrication of the MIP gripper, verify the mathematical model developed in Section III with experimental results, and conduct grasping and perching experiments to demonstrate the capability of the gripper.

Note that all experiments about the force measurement are conducted using a motorized test stand (ESM303, Mark-10), which can measure the force and displacement at the same time. For example, Fig. 9 shows the experimental setup for measuring the upward force with respect to displacement during P_{ch}.

A. Gripper Fabrication

The main design parameters of the gripper are listed in Table II. Most rigid parts (e.g., the fingers, extended fingers,

TABLE II
VALUE FOR GEOMETRIC PARAMETERS OF THE GRIPPER

parameter	symbol	value	unit
initial angle of torsion spring at J_1	ϕ_0	100	degree
angle between spring leg and a_3 at J_1	ϕ_e	28	degree
angle between horizontal line and LEF	θ_{e0}	93	degree
vertical distance between J_3 and J_2	$d_{(J_3, J_2)}$	0.5	mm
length between J_1 and J_2	l_{el}	34.0	mm
distance between J_2 and center line	d_{lef}	23.4	mm
length between J_3 and end of handle	l_f	31.5	mm
length between two handles at CJ	l_t	3.6	mm
length of handle at switch part	l_h	14.6	mm
width of impact pad	w_{sp}	30	mm
spring constant of beam	k_b	650	N/m
effective length of carbon fiber plates	l_{cb}	31	mm
spring constant of tube	k_θ	0.01647	N/rad
spring constant for springs at J_1	k_{s1}	0.0036	N/rad
spring constant for springs at J_2	k_{s2}	0.0036	N/rad

intermediate links, base, etc.) are 3-D printed (Ender-3 pro) with PLA materials. To generate reliable forces during bending and allow for length adjustment, the two vertical beams are carbon fiber plates (width × thickness: 7.9 × 0.8 mm, CF312032048, Goodwinds Composites LLC) as opposed to previous beams made from PLA [8]. To connect the plates to the fingers through joint J_3, two 3D printed beam heads are used. For the two CJs, the tube (ULTRA-C-062-3, Sain-Tech) has inner and outer diameters of 1.6 and 6.35 mm, respectively. The width of the impact pad w_{sp} should be close to two times of d_{lef} for blocking the two LEFs during P_{ch} (see Fig. 5). The spring constants used in our gripper are listed in Table II and discussed below.

1) *Linear spring constant k_b for beams:* Since the beam head (l_{bh}) is a part of beams during bending, k_b cannot be calculated from the carbon fiber plates' dimensions directly. Therefore, we experimentally obtain k_b with the length of l_{cb} from 25 to 33 mm. The experiment setup is shown at the bottom-left diagram of Fig. 8. We apply an upward force F to bend the beam. By recording and plotting F with respect to d_b, we can obtain the value of k_b for a given length l_{cb}. We conduct the experiments for different l_{cb} and plot the results in Fig. 8.
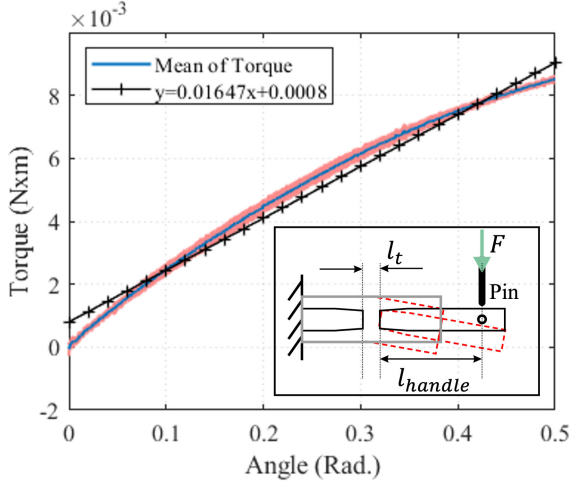
This article has been accepted for inclusion in a future issue of this journal. Content is final as presented, with the exception of pagination.

8

IEEE/ASME TRANSACTIONS ON MECHATRONICS

Fig. 10. Experimental results for the spring constants of the tube. The plot shows k_θ can be approximated as 0.01647 N/m. The red shaded area shows the standard deviation from three experiments. The experimental setup is shown inside the plot.

Fig. 11. Downward force F_d with respect to d during process P_{oc}. Different lengths of the carbon fiber plates l_{cb} are used: 25, 28, and 31 mm. Each shaded area shows the standard deviation from three repeated experiments.

2) *Torsion spring constant k_θ of CJs:* k_θ is also obtained by experiments. The experimental setup is shown at the bottom-right diagram of Fig. 10. We apply a downward force on the handle through a pin with the point touching on the handle as a free contact. This ensures that the moment arm is always constant. We can obtain and plot the bending angle and the corresponding torque, as shown in Fig. 10, from which we can approximate the torsion spring constant for CJs as $k_\theta = 0.01647$ N/rad.

3) Spring constant for torsion springs at J_1 and J_2 are both same $k_{s1} = k_{s2} = 0.0036$ N/rad (GT1206718-ML, Gardner Spring Inc). Note that we manually modify all the torsion springs to have an initial angle of 0°.

B. Profile of Downward Force $F_d(d)$ During P_{oc}

To verify $F_d(d)$ during process P_{oc}, we conduct three sets of experiments for three different lengths of the carbon fiber plates ($l_{cb} = 25$, 28, and 31 mm) by using the test stand to push the switch part and record both the force and displacement. Fig. 11 shows the comparison between the simulations and the experimental results. Note that the initial displacement d starts from 0 mm at S_o and gradually increases until F_d becomes 0 N, after which the bistable mechanism will automatically switch to the bottom stable state. From the plot, the downward force to close the gripper should be larger than 0.87, 0.65, and 0.42 N for $l_{cb} = 25$, 28, and 31 mm, respectively, in order to close the gripper. The mean error of the force between the simulations and the experiments with $l_{cb} = 25, 28$, and 31 mm are 0.28%, 3.99%, and 0.95%, respectively. As a result, the theoretical model can accurately predict the force. In this work, we select l_{cb} to be 31 mm for perching and grasping experiments. Therefore, the downward force should be greater than 0.42 N to close the gripper. The discrepancy between the simulations and experimental results after crossing the maximum of F_d is mainly because k_t of the CJs is considered as a constant in the simulation, but it will increase when a longitudinal force is applied to the tube,
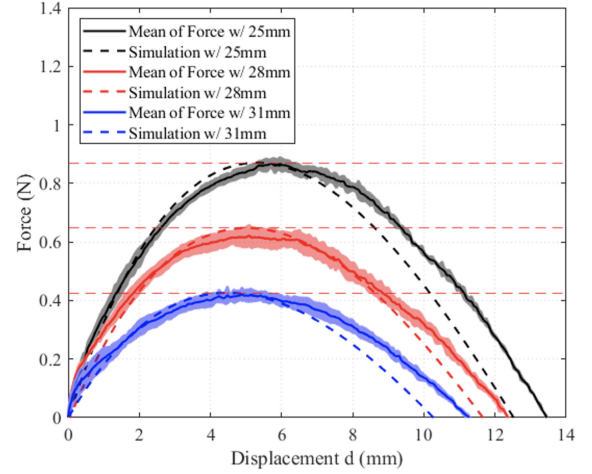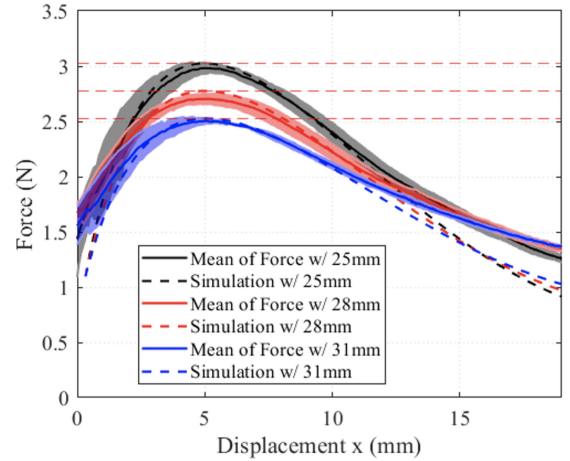

Fig. 12. Upward force F_u with respect to displacement x during P_{ch} with different l_{cb}: 25, 28, and 31 mm. Each shaded area shows the standard deviation from three experiments. The horizontal red dash lines show the maximum of F_u, which increases when l_{cb} decreases from 31 to 25 mm.

which is the case when d becomes larger since the bending of the vertical beam will generate a longitudinal force applied to the tube [8].

C. Profile of Upward Force $F_u(x)$ During P_{ch}

To verify $F_u(x)$ during the process P_{ch}, we also conduct three sets of experiments for three different lengths of the carbon fiber plates ($l_{cb} = 25$, 28, and 31 mm) by using the test stand (see Fig. 9). Fig. 12 shows the comparison between the simulation and experimental results of F_u with respect to x when $l_{cb} = 25$, 28, and 31 mm, respectively. The figure only shows when $x < 20$ mm since when $x > 20$ mm, the impact pad will prevent the two LEFs from moving (refer to the gripper design in Fig. 3). The mean errors of F_u between the simulations and experiments are 1.44%, 2.62%, and 0.83%, respectively, for $l_{cb} = 25, 28$, and 31 mm. From the figure, to successful switch the state from S_c
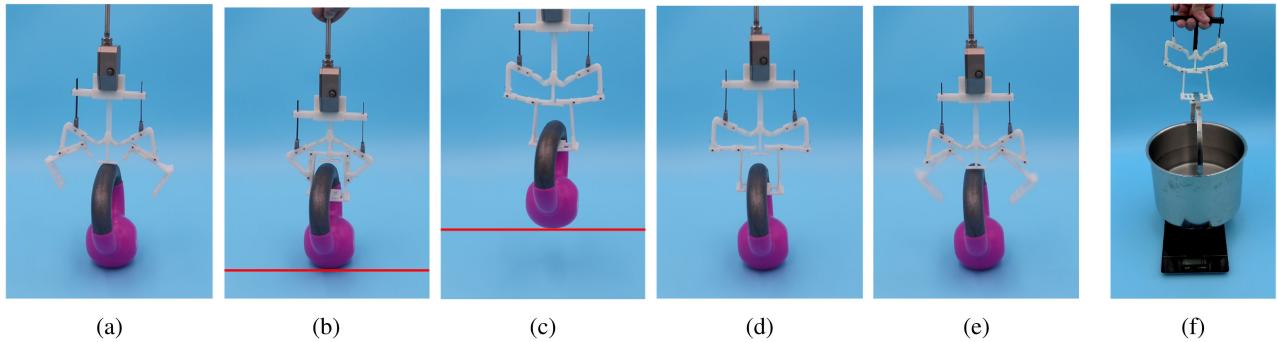
Fig. 13. Grasping experiment. (a) Gripper is open. (b) Gripper contacts the handle of the kettlebell (2.27 kg) to close. (c) Extended fingers keep the closed configuration and lift up the kettlebell. (d) Gripper moves down to put the kettlebell on the ground. (e) When the force is removed from the extended fingers, the gripper opens to release the kettlebell. (f) Gripper can lift up a bucket with water (3.7 kg).
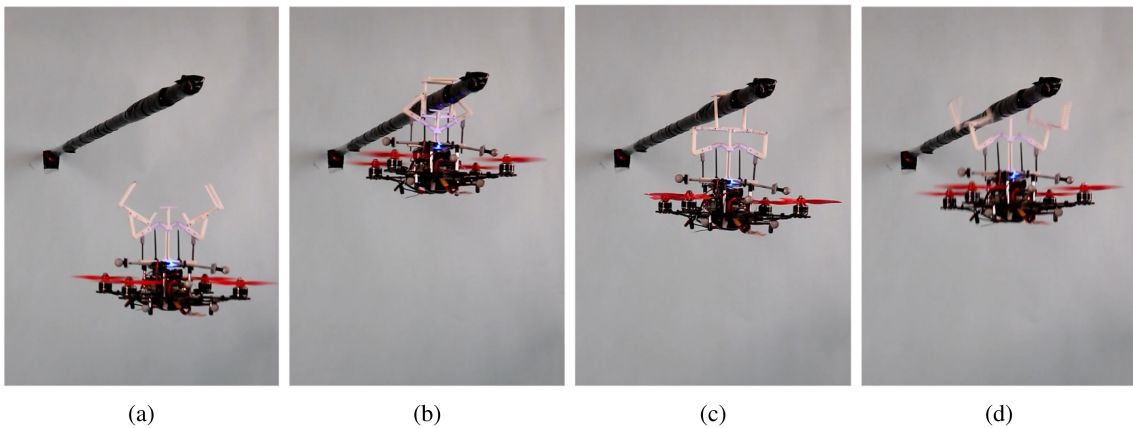

Fig. 14. Perching experiment. (a) Quadcopter flies under a rod while the gripper is open. (b) Gripper contacts the rod to close the gripper. (c) Quadcopter's mass switches the state of the bistable mechanism, but the two extended fingers remain closed to let the quadcopter hang on the rod. (d) Upward thrust opens the extended fingers to release the gripper from the rod, then the quadcopter can fly away.

to S_h, the upward force should be larger than the maximum of $F_u(x)$, i.e., 3.03 N, 2.78 N, and 2.53 N for $l_{cb} = 25$, 28, and 31 mm, respectively. This means if the gripper is used for perching, the total mass of the drone with the gripper should be larger than 2.53 N to allow successful passive opening when $l_{cb} = 31$ mm. Note that after passing the peak of F_u, there are discrepancies between the simulation and experiments, which should also be mainly due to the nonlinear stiffness of the tube as explained in Section IV-B.

D. Static Grasping Experiment

After verifying the model, we demonstrate that the MIP gripper can grasp different heavy objects: a kettlebell (2.27 kg) and a bucket with water (3.7 kg) in Fig. 13 (also see the Supplementary Material). The complete grasping process is demonstrated by grasping the kettlebell. The gripper is installed upside down [see Fig. 13(a)]. As the gripper moves down, its impact pad contacts the kettlebell to close the gripper [see Fig. 13(b)]. In the holding state, it can lift up the kettlebell [the red lines in Fig. 13(b) and (c)]. Once the gripper moves down until the kettlebell touches the ground, the closed extended fingers open automatically [see Fig. 13(d) and (e)]. Fig. 13(f) shows the gripper can grasp a

bucket of 3.7 kg with a thinner handle (the detailed process can be found in the Supplementary Material).

E. Perching Experiment

We also demonstrate aerial perching of a quadcopter with the MIP gripper. The gripper is fixed onto the top of a customized quadcopter developed in our lab (565 g without the gripper). The experimental results are illustrated in Fig. 14 (also see the Supplementary Material). The gripper is initially open [see Fig. 14(a)], and it closes upon contacting a fixed rod [see Fig. 14(b)]. After the propellers stop rotating, the mass of the quadcopter will be applied to the UEFs to switch the gripper to the holding state, and the quadcopter can rest on the rod [see Fig. 14(c)] without additional energy input. To release from the rod, we simply apply an upward thrust to remove the force applied on the UEFs of the gripper [see Fig. 14(d)].

F. Aerial Grasping Experiment

Finally, we demonstrate aerial grasping by attaching the gripper onto the bottom of the quadcopter (see Fig. 15, also see the Supplementary Material). Four legs are added to the

This article has been accepted for inclusion in a future issue of this journal. Content is final as presented, with the exception of pagination.

10   IEEE/ASME TRANSACTIONS ON MECHATRONICS
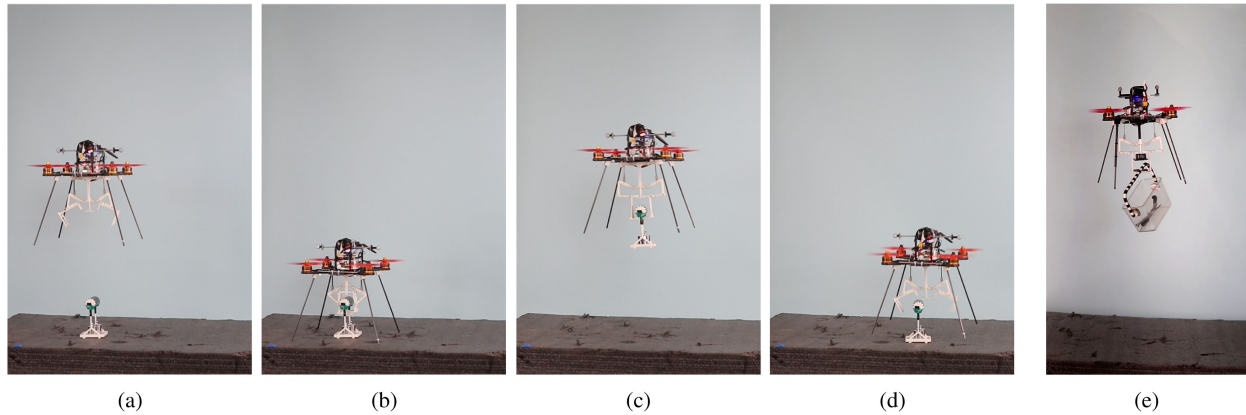
Fig. 15.   Aerial grasping experiments. (a) Gripper is open and fixed on bottom of the quadcopter. (b) Gripper contacts the handle of an object (260 g) and closes. (c) Gripper keeps the holding state and lifts up the object when the quadcopter flies up. (d) Once the quadcopter lands on the ground, the force applied on the extended fingers is removed, the extended fingers will open to release the object. (e) Griper can grasp a container with a handle (225 g) without landing on the ground.

quadcopter to protect and leave space for the gripper. The target object is 260 g in total and has a handle to facilitate grasping. The quadcopter flies over the object [see Fig. 15(a)]. Once the quadcopter moves down to let the gripper's impact pad touch the handle, the impact force will close the gripper [see Fig. 15(b)]. Then, the quadcopter flies up, and the gripper switches to a holding state when the object is lifted up [see Fig. 15(c)]. After the quadcopter carries the object in flight, the quadcopter lands, releasing the object [see Fig. 15(d) and (e)]. In addition to this object, we also demonstrate that the gripper can be used for grasping a box with a thin handle (225 g) without landing on the ground during the grasping process, as shown in Fig. 15(e) (the detailed process can be found in the Supplementary Material).

V. DISCUSSIONS

As demonstrated in our experiment, the MIP gripper is purely passive without any actuator, yet it can be used for both aerial grasping and perching. The MIP gripper with a mass of 28 g can lift up a mass of 3.7 kg under a static condition: more than 132 times its own mass. Note that a dynamic load could reduce the ratio, and if it is used to lift a mass larger than 3.7 kg, the gripper might break at some locations: the grids at the UEF, joint J_2, or the connection between beam head and the beam. However, we believe it can hold even heavier weights if we strengthen those critical parts. This means that it can be used for perching or grasping for heavy drones. Because it does not have any actuator, it can be fabricated at a low cost (we estimate the gripper costs around $4). Because of its mechanical intelligence, it does not need precise position control, alleviating the requirement for computational intelligence. In this case, we believe it can be used for rapidly grasping an object in flight without sophisticated control [22]. We envision that it can be installed on commercially available quadcopters to enable the perching/grasping capability. It can also be added to the end of existing aerial manipulators [25] to facilitate manipulation tasks.

Using the gripper for perching or grasping, we need to pay attention to the following aspects. First, the gripper currently only works for rod-like objects, whose size should be smaller than the width of the UEF. If an object is too large, the latch may not be able to insert into the grid of the UEFs, preventing the extended fingers from keeping the closed state when an upper force is applied. To address this issue, we might need to replace the rigid UEFs with some compliant bistable strips [26]. Besides rod-like objects, we believe a similar mechanism should work for perching onto surfaces [10] by attaching a vacuum pad at the end. Second, for grasping tasks, the mass of the object should be large enough to ensure a successful state transition from S_c to S_h. In this case, the drone may not be able to grasp a lightweight object (i.e., it might be impossible to find a valid range for k_b given the object's mass). To solve this problem, we can exploit the upward acceleration of the drone to ensure a sufficient F_u for a successful state transition. Third, also for grasping, the height of objects should be large enough to allow the gripper to enclose the rod on the object. Finally, since no actuator is used for the gripper, we need to ensure that there will be an object enclosed inside the extended finger from S_o to S_c. Otherwise, the gripper will need to be manually reset to S_o.

VI. CONCLUSION

In this work, we designed, analyzed, and characterized an MIP gripper for aerial perching and grasping. Initially open, the gripper can close by utilizing the impact force between the gripper and an object, hold the closed configuration by external weights, and automatically open when weights are removed. We established models that can accurately predict the required force to open or close the gripper. Based on the models, we also establish design guidelines for the gripper to ensure successful perching/grasping. Various experiments are conducted to demonstrate aerial perching and grasping by placing the gripper onto a quadcopter. Since the gripper is lightweight compared

with the quadcopter (up to 0.75%), we expect the MIP gripper to be ideal for aerial perching to enable long-duration monitoring tasks and aerial grasping to carry heavy payloads.
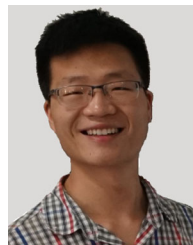
REFERENCES

[1] W. R. Roderick, M. R. Cutkosky, and D. Lentink, "Touchdown to take-off: At the interface of flight and surface locomotion," *Interface focus*, vol. 7, no. 1, 2017, Art. no. 20160094.

[2] P. Liu, S. P. Sane, J.-M. Mongeau, J. Zhao, and B. Cheng, "Flies land upside down on a ceiling using rapid visually mediated rotational maneuvers," *Sci. Adv.*, vol. 5, no. 10, 2019, Art. no. eaax1877.

[3] K. Hang *et al.*, "Perching and resting–A paradigm for UAV maneuvering with modularized landing gears," *Sci. Robot.*, vol. 4, no. 28, 2019, Art. no. eaau6637.

[4] J. Thomas *et al.*, "Aggressive flight with quadrotors for perching on inclined surfaces," *J. Mechanisms Robot.*, vol. 8, no. 5, 2016, Art. no. 051007.

[5] H. Zhang, B. Cheng, and J. Zhao, "Optimal trajectory generation for time-to-contact based aerial robotic perching," *Bioinspiration biomimetics*, vol. 14, no. 1, 2018, Art. no. 016008.

[6] M. Sitti, "Physical intelligence as a new paradigm," *Extreme Mechanics Lett.*, vol. 46, 2021, Art. no. 101340.

[7] M. Kovac, "Learning from nature how to land aerial robots," *Science*, vol. 352, no. 6288, pp. 895–896, 2016.

[8] H. Zhang, E. Lerner, B. Cheng, and J. Zhao, "Compliant bistable grippers enable passive perching for micro aerial vehicles," *IEEE/ASME Trans. Mechatronics*, vol. 26, no. 5, pp. 2316–2326, Oct. 2021.

[9] D. Howard, A. E. Eiben, D. F. Kennedy, J.-B. Mouret, P. Valencia, and D. Winkler, "Evolving embodied intelligence from materials to machines," *Nature Mach. Intell.*, vol. 1, no. 1, pp. 12–19, 2019.

[10] M. T. Pope *et al.*, "A multimodal robot for perching and climbing on vertical outdoor surfaces," *IEEE Trans. Robot.*, vol. 33, no. 1, pp. 38–48, Feb. 2017.

[11] W. Chi, K. Low, K. H. Hoon, and J. Tang, "An optimized perching mechanism for autonomous perching with a quadrotor," in *Proc. IEEE Int. Conf. Robot. Automat.*, 2014, pp. 3109–3115.

[12] K. M. Popek *et al.*, "Autonomous grasping robotic aerial system for perching (agrasp)," in *Proc. IEEE/RSJ Int. Conf. Intell. Robots Syst.*, 2018, pp. 1–9.

[13] U. A. Fiaz, M. Abdelkader, and J. S. Shamma, "An intelligent gripper design for autonomous aerial transport with passive magnetic grasping and dual-impulsive release," in *Proc. IEEE/ASME Int. Conf. Adv. Intell. Mechatronics*, 2018, pp. 1027–1032.

[14] P. M. Nadan *et al.*, "A bird-inspired perching landing gear system," *J. Mechanisms Robot.*, vol. 11, no. 6, 2019, Art. no. 061002.

[15] A. McLaren, Z. Fitzgerald, G. Gao, and M. Liarokapis, "A passive closing, tendon driven, adaptive robot hand for ultra-fast, aerial grasping and perching," in *Proc. IEEE/RSJ Int. Conf. Intell. Robots Syst.*, 2019, pp. 5602–5607.

[16] C. C. Kessens, J. Thomas, J. P. Desai, and V. Kumar, "Versatile aerial grasping using self-sealing suction," in *Proc. IEEE Int. Conf. Robot. Automat.*, 2016, pp. 3249–3254.

[17] C. E. Doyle *et al.*, "An avian-inspired passive mechanism for quadrotor perching," *IEEE/ASME Trans. Mechatronics*, vol. 18, no. 2, pp. 506–517, Apr. 2013.

[18] M. L. Burroughs, K. Beauwen Freckleton, J. J. Abbott, and M. A. Minor, "A sarrus-based passive mechanism for rotorcraft perching," *J. Mechanisms Robot.*, vol. 8, no. 1, 2016, Art. no. 011010.

[19] D. J. Dunlop and M. A. Minor, "Modeling and simulation of perching with a quadrotor aerial robot with passive bio-inspired legs and feet," *ASME Lett. Dyn. Syst. Control*, vol. 1, no. 2, 2021, Art. no. 021005.

[20] H.-N. Nguyen, R. Siddall, B. Stephens, A. Navarro-Rubio, and M. Kovač, "A passively adaptive microspine grapple for robust, controllable perching," in *Proc. 2nd IEEE Int. Conf. Soft Robot.*, 2019, pp. 80–87.

[21] W. Stewart, L. Guarino, Y. Piskarev, and D. Floreano, "Passive perching with energy storage for winged aerial robots," *Adv. Intell. Syst.*, 2021, Art. no. 2100150.

[22] J. Fishman, S. Ubellacker, N. Hughes, and L. Carlone, "Dynamic grasping with a" soft" drone: From theory to practice," *IEEE/RSJ Int. Conf. Intell. Robots Syst.*, 2021, pp. 4214–4221.

[23] H. Zhang, J. Sun, and J. Zhao, "Compliant bistable gripper for aerial perching and grasping," in *Proc. Int. Conf. Robot. Automat.*, 2019, pp. 1248–1253.

[24] L. Cao, A. T. Dolovich, A. L. Schwab, J. L. Herder, and W. Zhang, "Toward a unified design approach for both compliant mechanisms and rigid-body mechanisms: Module optimization," *J. Mech. Des.*, vol. 137, no. 12, 2015, Art. no. 122301.

[25] F. Ruggiero, V. Lippiello, and A. Ollero, "Aerial manipulation: A literature review," *IEEE Robot. Automat. Lett.*, vol. 3, no. 3, pp. 1957–1964, Jul. 2018.

[26] R. Jitosho, K. Choi, A. Foris, and A. Mazumdar, "Exploiting bistability for high force density reflexive gripping," in *Proc. Int. Conf. Robot. Automat.*, pp. 1241–1247, 2019.

HaoTse Hsiao received the B.S. degree in physics and the M.S. degree in optoelectronic engineering from National Dong Hwa University, Hualien, Taiwan, in 2012 and 2014, respectively. He is currently working toward the M.S. degree in computer engineering with Colorado State University, Fort Collins, CO, USA.

His current research interests include bistable grippers and flying robots.

Jiefeng Sun (Student Member, IEEE) received the B.S. degree in mechanical engineering from the Lanzhou University of Technology, Lanzhou, China, in 2014, and the M.S. degree in mechanical engineering from the Dalian University of Technology, Dalian, China, in 2017. He is currently working toward the Ph.D. degree in mechanical engineering with Colorado State University, Fort Collins, CO, USA.

His current research interests include artificial muscle, soft robots, and reconfigurable robots.

Haijie Zhang received the B.S. degree in electrical engineering from the School of Automation, Harbin Engineering University, Harbin, China, in 2014, and the Ph.D. degree in mechanical engineering from Colorado State University, Fort Collins, CO, USA, in 2021.

He is currently a Data Scientist with Change Healthcare. His research interests include vision based control and flying robots.

Jianguo Zhao (Member, IEEE) received the B.E. degree in mechanical engineering from the Harbin Institute of Technology, Harbin, China, in 2005, the M.E. degree in mechatronic engineering from the Shenzhen Graduate School, Harbin Institute of Technology, Shenzhen, China, in 2007, and the Ph.D. degree in electrical engineering from Michigan State University, East Lansing, MI, USA, in 2015.

He is currently an Associate Professor with Colorado State University, Fort Collins, CO, USA, and the Director of Adaptive Robotics Lab. His research interests include soft robots, flying robots, and reconfigurable robots.

He is currently a Technical Editor of the IEEE/ASME TRANSACTIONS ON MECHATRONICS.